Analysis of the frequency dependent gate capacitance in CNTFETs

Martin Claus[*], Stefan Blawid[†], Paulius Sakalas[*] and Michael Schröter[*,‡]

[*] Department of Electrical Engineering and Information Technology
Technische Universität Dresden, Germany, Email: martin.claus@tu-dresden.de
[†] Department of Electrical Engineering, Universidade de Brasília, Brazil, Email: stefan@ene.unb.br
[‡] ECE Department, UC San Diego, USA, Email: mschroter@ieee.org

Abstract—A time-dependent effective-mass Schrödinger-Poisson solver is used to study the frequency dependence of the gate capacitance of a short Schottky-barrier carbon nanotube field-effect transistor (CNTFET). A delayed (re)charging of the channel causes a (non-quasi-static) drop of the gate capacitance for higher frequencies on a characteristic scale, which can be related to the escape time of the carriers. The impact of Schottky-barriers on the escape time is discussed both analytically and by means of transient simulations. A comparison with experimental data reveals an interesting qualitative similarity.

Index Terms—CNTFET, ballistic transport, high-frequency behavior, gate capacitance, double barrier structure, non-quasi-static phenomena, escape time

I. INTRODUCTION

Recent experimental results of prototype CNTFETs [1] and first circuit design studies [2] based on a production-type CNTFET technology [3] indicate that the CNTFET technology may be a potential alternative to existing semiconductor process technologies especially for high-frequency (HF) analog applications. However, the understanding of HF phenomena in CNTFETs is still quite limited for two reasons: (*i*) experimental HF characterization of single-tube (ST) FETs is almost impossible due to their relatively high parasitics and very high impedance level compared to the standardized $50\,\Omega$ measurement systems, and (*ii*) HF simulation capabilities are restricted to (short channel) ST devices and rely on non-verified assumptions concerning the transient modeling. Thus, only a few publications [4]–[9] study the small-signal HF behavior of CNTFETs which is commonly described by two-port S- or Y-parameters.

On the other hand, experimental HF characterization of multi-tube (MT) CNTFETs is possible and results are shown in the present paper. A decrease of the gate capacitance $\tilde{C}_{\mathrm{gg}}$ for frequencies well below $10\,\mathrm{GHz}$ ($V_{\mathrm{ds}} = 0\,\mathrm{V}$) for a Schottky-barrier (SB) MT CNTFET is observed. This frequency scale should also be predicted by simulations. One should keep in mind, however, that MT CNTFETs have some fabrication related unique properties, such as parasitic metallic tubes within the channel and intertube crossings, which can not be explained on a ST level (see [10] for an overview on state-of-the-art CNTFET technology).

The speed of a CNTFET is limited, among others, by the time required to charge or discharge the tube. The charging time is traditionally associated with the transit of the carriers through the channel. Semi-classically, a thermionically injected carrier with a mean velocity $v_{\mathrm{avg}} = 2{\times}10^7\mathrm{cm/s} < v_{\mathrm{F}} = 8{\times}10^7\mathrm{cm/s}$ needs only $2\,\mathrm{ps}$ to cross half of a typically $800\,\mathrm{nm}$ long channel (injection from both contacts at zero V_{ds}), which would lead to characteristic frequencies well above $500\,\mathrm{GHz}$. The interesting question arises if the discrepancy between the measurements and flight-time estimations can already be explained with the impact of potential barriers. Especially in short SB CNTFETs the build up of resonant tunneling charges is delayed, which is the focus of the present study. Randomly crossing CNTs may cause additional small barriers in a longer channel and possibly slow down the channel recharging even further.

The present study is structured as follows. First, the frequency dependence of the gate capacitance of a short ballistic SB CNTFET is numerically calculated and explained. For the simulation study in this paper, a recently published ballistic effective-mass Schrödinger-Poisson solver [9] is used which allows the simulation of time-dependent transport based on coherent quantum-ballistic charge injection. The relevant time scale for the HF response of a ballistic device can be determined from the escape time of the injected carriers:

$$t_{\mathrm{Esc}} = \hbar/\Gamma, \qquad (1)$$

as already concluded in [9]. Here Γ is the (averaged) width of the resonances in the transmission spectrum. The escape time is further analyzed for the case of charge injection into a simplified transistor channel described by a (non-self-consistent) double barrier structure (DBS). Analytical equations are derived, which allow to study the impact of SBs and the extrapolation to longer channels. Finally, we return to the experimental results and compare our findings to the frequency dependent gate capacitance of a long MT CNTFET.

II. TRANSIENT DEVICE SIMULATION

The method proposed in [11] is used to extract the $\tilde{Y}$-parameters of a common source fully gated $50\,\mathrm{nm}$ long CNTFET by transient step excitation ($V_{\mathrm{step}} = 1\,\mathrm{mV}$) of the device terminals with respect to a given bias point followed by Fourier decomposition.

The gate capacitance $\tilde{C}_{\mathrm{gg}}$ is extracted from the time-dependent simulations as $\tilde{C}_{\mathrm{gg}} = \mathrm{Im}\left\{\tilde{Y}_{\mathrm{gg}}\right\}/(2\pi f)$ which

approaches its quasi-static limit $C_{gg} = dq_{ch}/dV_{gs}$ for $f \to 0$ (q_{ch} is the channel charge). The frequency-dependence of $\tilde{C}_{gg}$ for zero V_{ds} is shown in Fig. 1. Obviously, the higher the frequency, the lower is the value of $\tilde{C}_{gg}$. Other HF characteristics are discussed in [9].
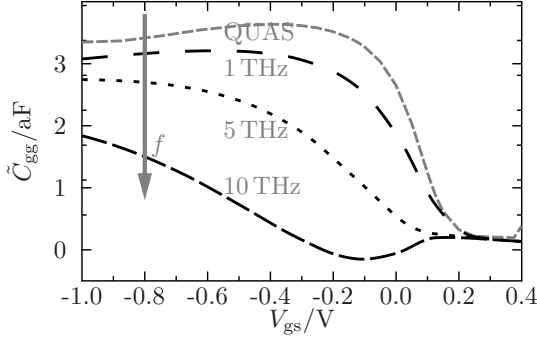

Fig. 1: Total gate capacitance $\tilde{C}_{gg}$ as function of the gate voltage V_{gs} for $V_{ds} = 0$ and several frequencies. The simulation and device parameters are identical to the parameters in [9].

The frequency dependence of $\tilde{C}_{gg}$ can be explained as follows: A zero-order approximation of the total gate capacitance is $C_{gg} = C_{ox}C_q/(C_{ox} + C_q)$ where C_{ox} is the oxide capacitance and C_q is the quantum capacitance (change of channel charge with respect to changes of the electrostatic tube potential ψ_{ch}). Since C_{ox} is frequency-independent (at least in the simulation), the frequency dependence of C_{gg} is due to C_q which thus decreases with frequency. The related decrease of the change of the charge carrier concentration Δp with frequency is shown in Fig. 2. (Δp is extracted from the time-dependent simulations in a similar manner as the Y-parameters). As the change of the carrier concentration
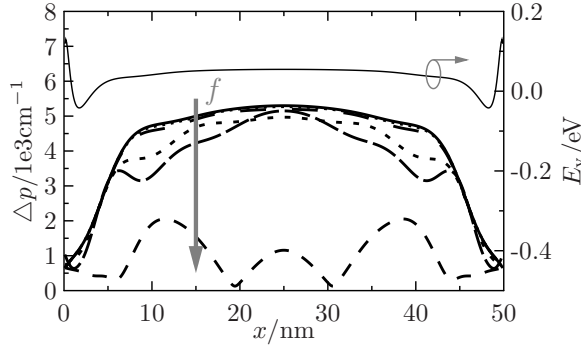

Fig. 2: Change of the hole concentration Δp along the channel as response to sinusoidal gate signals ($v_{gs} = 1\,\mathrm{mV}$) for $f = 0, 1, 5, 10$ and $50\,\mathrm{THz}$ and $V_{gs} = -0.5\,\mathrm{V}$, $V_{ds} = 0\,\mathrm{V}$. The quasi-static ($f = 0\,\mathrm{Hz}$) value of Δp is derived from two steady-state simulations with corresponding bias points. The valence band edge E_v of the first subband is also shown.

decreases with frequency, the change of the electrostatic potential increases due to self-consistency (in the zero-order model $\triangle\psi_{ch} = C_{gg}/C_q v_{gs}$) and approaches finally for highest

frequencies the change of the gate potential (not shown). For comparisons with experiments (see Fig. 6), we employ the zero-order model to approximately calculate the quasi-static value of C_q from the (measured/simulated) value C_{gg} modeling C_{ox} as the capacitance of a cylinder-plate geometry, yielding for the here simulated device $C_q/l_g = 0.13\,\mathrm{aF/nm}$.

Following the above arguments, the frequency dependence of $\tilde{C}_{gg}$ is due to a significant weaker change of the carrier concentration within the channel for higher frequencies, i. e. a pronounced recharging delay. The delay may be explained as follows: The valence band within the channel of the CNTFET forms a symmetric DBS (see Fig. 2) for $V_{ds} = 0$. Thus, (*i*) carriers must traverse the SBs (33% of the carriers in the channel tunnel through the SBs) to recharge the channel, and (*ii*) carrier injection is dominant for energies which are very close to the energies of the resonant states of the DBS otherwise the carriers are totally reflected. Hence, as a relevant time scale for the carrier traversal time we may consider the escape time of the carriers which can be read off from the widths Γ of the resonances in the transmission spectrum. A typical average value is in the order of $3\,\mathrm{meV}$ for the given device. The escape time then equals roughly $0.22\,\mathrm{ps}$ which is comparable to the cycle duration of a gate signal frequency of $4.5\,\mathrm{THz}$. Charge carriers cannot follow faster oscillations and the change of the carrier concentration is suppressed. Therefore, the escape frequency (a DC property influenced e. g. by Schottky and/or potential barriers near the contacts) sets a typical scale for the decrease of the gate capacitance as seen in Fig. 1.

The undulatory profile of the carrier concentration (and the electrostatic potential) for higher frequencies visible in Fig. 2 is a consequence of the fact that the transmission spectrum comprises resonances of different widths. Thus, narrow resonance states (at low energies) may be left empty while an injection into wider resonance states (at higher energies) is still possible at high frequencies. However, empty states lead to undulatory profiles.

III. CHARGE INJECTION INTO A DBS

If a CNTFET is biased at $V_{ds} = 0\,\mathrm{V}$ the valence band in the channel region can be approximated as a double barrier structure (DBS). This motivates us to (re)investigate charge injection into a simplified DBS as shown in the inset of Fig. 3, where rectangular potential barriers ($\Phi_{sb} = 0.25\,\mathrm{eV}$, $m_{cnt} = 0.05m_0$) are used to mimic the impact of the SBs. Fig. 3 also shows the transmission probability of the DBS near one resonant energy E_r. Following the supposition drawn from the transient device simulations in the previous section, the corresponding escape frequency may set the scale for the non-quasi-static decrease of the gate capacitance.

The full width $\Gamma = \Gamma_1 + \Gamma_2$ of a transmission resonance at half maximum in the transmission peak can be determined from the individual transmission probabilities $\mathcal{T}_i$ through the individual barriers of the structure [12],

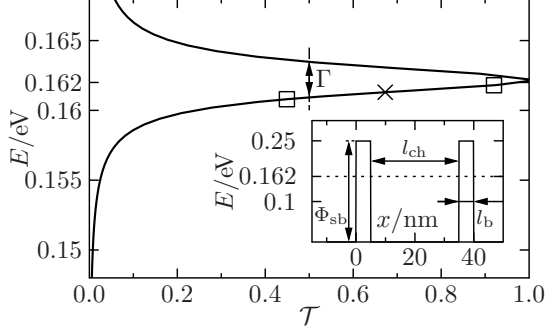$$\frac{\Gamma_i}{\hbar} = \frac{1}{\alpha l_{ch}} v_g \mathcal{T}_i = \frac{1}{t_{Esc}}, \tag{2}$$

Fig. 3: Transmission resonance for a simplified band profile (shown in the inset) for a SB width l_b of $5\,\text{nm}$.

Fig. 4: Channel length dependence of the escape frequency f_{Esc} and of the peak energy E_{reso} for the resonance shown in Fig. 3. Each barrier is $5\,\text{nm}$ long. The inset shows the barrier width dependence of f_{Esc} for two different channel lengths: numerical results (symbols) and analytical approximation for $l_{ch} = 30\,\text{nm}$ (solid line) and $50\,\text{nm}$ (dashed line).

where v_g is the band structure dependent group velocity $v_g = \frac{1}{\hbar}\frac{dE}{dk}$ and α is a fitting parameter including any phase shift associated with reflections at the barriers which had been neglected in the derivation. v_g and $\mathcal{T}_i$ are evaluated for an energy $E_{inj} \approx E_r$ (see below). According to (1), the escape frequency $f_{Esc} = 1/t_{Esc}$ is then given by

$$f_{Esc} = \frac{2}{\alpha l_{ch}} \exp(-2k(E_{inj})l_b)\sqrt{\frac{2}{m_{cnt}}E_{inj}} \qquad (3)$$

for a parabolic band structure with an effective mass m_{cnt} and a WKB approximation of the individual transmission probability through a rectangular barrier of length l_b. The momentum k in equation (3) is given by

$$k(E) = \sqrt{\frac{2m_{cnt}}{\hbar}(q\Phi_{sb} - E)}. \qquad (4)$$

Fig. 4 compares the escape frequency $f_{Esc,num}$ extracted from non-self-consistent numerical simulation solving the steady-state effective-mass Schrödinger equation [9] and the analytical approximation $f_{Esc,analy}$ given by equation (3) for different channel lengths l_{ch}. The energy E_{inj} is chosen to lie on the lower edge of the transmission resonance close to E_r (which changes with l_{ch}). The agreement is excellent for $\alpha = 0.6$. Note, that f_{Esc} drops from THz to few tens of GHz when changing the channel length from $50\,\text{nm}$ to $800\,\text{nm}$.

Eq. (3) also allows to study the impact of the SB width l_b on the escape frequency. The inset in Fig. 4 compares numerical simulation results with analytical results for $\alpha = 0.6$. The escape frequency for thin barriers can be estimated from the velocity v_r at resonance $f_{Esc} \approx 1.67 v_r \left(2/l_{ch}\right)$. For thicker barriers, however, the flight-time estimation fails and f_{Esc} is reduced exponentially with l_b, down to a few tens of GHz for long channels and reasonable values of the barrier widths.

The time-dependent simulation results shown in Fig. 5 confirm that resonant tunneling electrons cannot follow too rapid potential changes in a DBS. For several SB widths, the difference $\triangle|\phi(t)|^2 = |\phi(t)|^2 - |\phi_{ss}|^2$ between the time-dependent probability density $|\phi(t)|^2$ and the corresponding steady-state value $|\phi_{ss}|^2$ is calculated non-self-consistently with a time-dependent effective-mass Schrödinger equation [9] for an oscillating potential well with a frequency of $500\,\text{GHz}$
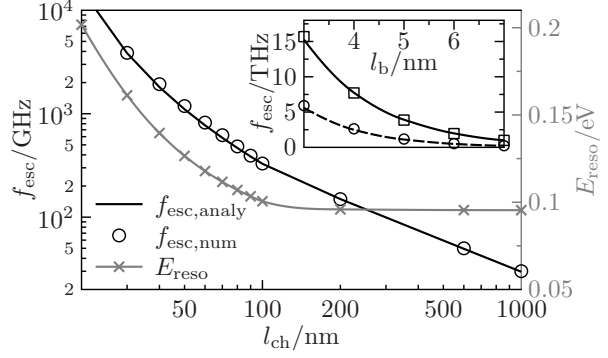
and an amplitude of $0.5\,\text{meV}$. The injection energy equals E_{inj} shown in Fig. 4. The difference $\triangle|\phi(t)|^2$ is shown at $1/8$ (dashed line) and $1/4$ (solid line) of the barrier oscillation cycle time. For comparison, Fig. 5 also shows the differences $|\phi_{max/min}|^2 - |\phi_{ss}|^2$. Here, the steady-state probability densities $|\phi_{max}|^2$ and $|\phi_{min}|^2$ are calculated for the maximal and minimal barrier height corresponding to $1/4$ (circles) and $3/4$ (squares) of the oscillation cycle time T, respectively.

Obviously, for thin barriers, $\triangle|\phi(t = T/4)|^2$ equals the quasi-static value $|\phi_{max}|^2 - |\phi_{ss}|^2$. However for $l_b = 7\,\text{nm}$, $|\phi(t)|^2$ is almost time-invariant and equals $|\phi_{ss}|^2$ leading to a vanishing $\triangle|\phi(t)|^2$, i.e. a recharge is suppressed. The simulation results for $l_b = 5\,\text{nm}$ demonstrate that for the simplified DBS already for frequencies well below f_{Esc} the injected wave function does not reach the steady-state values. Thus, even below f_{Esc}, the carrier concentration within the channel cannot follow oscillations of the potential well and the associated gate capacitance becomes frequency-dependent.
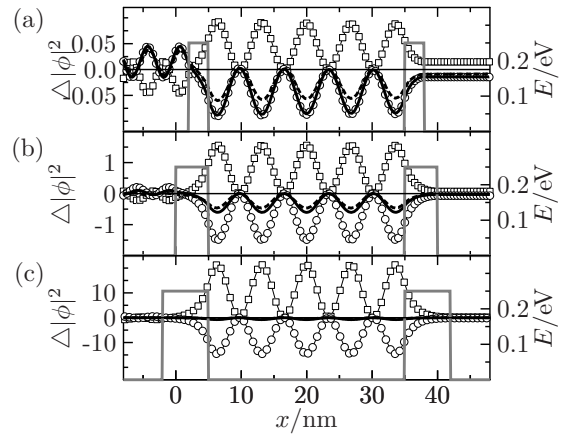

Fig. 5: Time-dependence of an injected wave for an oscillating potential well with $500\,\text{GHz}$ and different SB widths.

IV. DISCUSSION AND CONCLUSION

In the shown transient simulations of a short ballistic ST CNTFET the frequency dependence of the gate capacitance at $V_{ds} = 0\,V$ can be traced to a drop of the quantum capacitance for frequencies slightly below the escape frequency of resonant tunneling charge carriers. This observation is plausible because resonant tunneling carriers spend a longer time (proportional to the inverse resonance width Γ^{-1}) in the transistor channel and contribute most significantly to the quasi-static capacitance value. However, for too rapid gate oscillations the carriers cannot follow and the pile up of charge due to resonant tunneling will be suppressed, as we have demonstrated for a simplified DBS, and the gate capacitance eventually decreases.

The times involved are considerably longer than estimated from flight times employing the Fermi velocity or a (reasonably) reduced mean velocity due to scattering. Especially, for $V_{ds} = 0\,V$, the escape times are large due to the Schottky-barriers at both sides of the channel.

It is interesting to note that the frequency-dependence of $\tilde{C}_{gg}$ is qualitatively similar to experimental results for the intrinsic gate capacitance C_{gg} of a MT, multi-finger top-gated SB CNT-FET shown in Fig. 6. The channel comprises approximately $n_t = 3000$ semiconducting and metallic $800\,nm$ long tubes in parallel (for more information on the technologie see [3]). For de-embedding the gate capacitance, an open structure is used that is identical to the transistor structure without tubes. A pronounced decrease of C_{gg} for frequencies well below $10\,GHz$ is observed.

The derived quasi-static quantum capacitance (following the procedure given in Sec. III) is twice as large as the simulated one, which seems reasonable considering the neglect of scattering and inter-tube crossings, which also will affect the frequency response. Therefore, in spite of the qualitative similarity of the experimental data and the simulation results, the applicability of the employed model to explain the observed frequency scale remains questionable. Although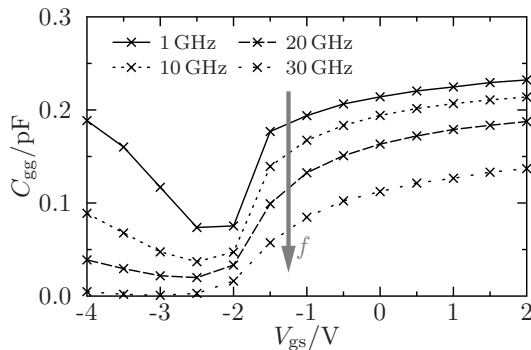 scattering times in CNTFETs are long due to the restricted phase space, phonon scattering is not negligible for realistic device dimensions and leads at least to an increased quasi-static value of the quantum capacitance [13]. Furthermore, phonon scattering will destroy coherence and impacts resonant tunneling [14], [15], but the consequences for the transient behavior are less clear. However, for the simplified DBS, escape frequencies of a few tens of GHz are easily conceivable. Therefore, the DBS may be also an effective model describing the impact of small barriers within the channel due to inter-tube crossing in MT CNTFETs. Investigating such a structure and the influence of scattering is left to further studies.

REFERENCES

[1] L. Nougaret, H. Happy, G. Dambrine, V. Derycke, J. P. Bourgoin, A. A. Green, and M. C. Hersam, "80 GHz field-effect transistors produced using high purity semiconducting single-walled carbon nanotubes," *Applied Physics Letters*, vol. 94, no. 24, p. 243505, 2009.

[2] M. Eron, S. Lin, D. Wang, M. Schroter, and P. Kempf, "An L-band carbon nanotube transistor amplifier," *Electronics Letters*, vol. 47, no. 4, pp. 265–266, 2011.

[3] M. Schroter, P. Kolev, D. Wang, S. Lin, N. Samarakone, M. Bronikowski, Z. Yu, P. Sampat, P. Syams, and S. McKernan, "A 4" Wafer Photostepper-Based Carbon Nanotube FET Technology for RF Applications," in *IEEE MTT-S International Microwave Symposium*, 2011.

[4] Y. Chen, Y. Ouyang, J. Guo, and T. X. Wu, "Time-dependent quantum transport and nonquasistatic effects in carbon nanotube transistors," *Applied Physics Letters*, vol. 89, no. 20, p. 203122, 2006.

[5] S. Ilani, L. A. K. Donev, M. Kindermann, and P. L. McEuen, "Measurement of the quantum capacitance of interacting electrons in carbon nanotubes," *Nature Physics*, vol. 2, no. 10, pp. 687–691, 2006.

[6] M. Claus, S. Mothes, and M. Schröter, "Modeling of NQS effects in carbon nanotube transistors," in *Proc. SISPAD*, Bologna, Italy, 2010, pp. 203–206.

[7] D. Kienle, M. Vaidyanathan, and F. Léonard, "Self-consistent ac quantum transport using nonequilibrium green functions," *Phys. Rev. B*, vol. 81, p. 115455, 2010.

[8] N. Paydavosi, A. U. Alam, S. Ahmed, K. D. Holland, J. P. Rebstock, and M. Vaidyanathan, "Rf performance potential of array-based carbon-nanotube transistors;part i: Intrinsic results," *IEEE Trans. on Electron Devices*, vol. 58, no. 7, pp. 1928–1940, july 2011.

[9] M. Claus, S. Blawid, S. Mothes, and M. Schröter, "High-frequency ballistic transport phenomena in schottky-barrier cntfets," *acc. for publication in Trans. on Electron Devices*, 2012.

[10] M. Schroter, M. Claus, P. Sakalas, D. Wang, and M. Haferlach, "An overview on the state-of-the-art of carbon-based radio-frequency electronics (invited paper)," in *BCTM*, 2012.

[11] S. E. Laux, "Techniques for small-signal analysis of semiconductor devices," *IEEE Trans. on Computer-Aided Design of Integrated Circuits and Systems*, vol. 4, no. 4, pp. 472–481, October 1985.

[12] S. Datta, *Electronic Transport in Mesoscopic Systems*, 7th ed. Cambridge University Press, 2007.

[13] Y. Yoon, Y. Ouyang, and J. Guo, "Effect of phonon scattering on intrinsic delay and cutoff frequency of carbon nanotube fets," *IEEE Trans. on Electron Devices*, vol. 53, no. 10, pp. 2467–2470, 2006.

[14] A. D. Stone and P. A. Lee, "Effect of inelastic processes on resonant tunneling in one dimension," *Phys. Rev. Lett.*, vol. 54, pp. 1196–1199, Mar 1985.

[15] M. Jonson and A. Grincwajg, "Effect of inelastic scattering on resonant and sequential tunneling in double barrier heterostructures," *Applied Physics Letters*, vol. 51, no. 21, pp. 1729–1731, 1987.

Fig. 6: Experimental data of the gate capacitance C_{gg} of a $800\,nm$ long MTSB CNTFET. At low frequencies $C_q/l_g n_t \approx 0.25\,aF/nm$ wich agrees well with [5] ($0.26\,aF/nm$).